munohistochemical study showed an abnormal accumulation of pCREB in GVD granules in hippocampal neurons of AD brains. These observations suggest that aberrant CREB-mediated gene regulation serves as a molecular biomarker of AD-related pathological processes, and support the hypothesis that sequestration of pCREB in GVD granules is in part responsible for deregulation of CREB-mediated gene expression in AD hippocampus.

5. Supplemental Material

Supplemental figures and tables can be found on http://www.my-pharm.ac.jp/~satoj/sub19.html as downloadable PDF files.

Acknowledegements

Human brain tissues were provided by Research Resource Network (RRN), Japan. This work was supported by a research grant to J-IS from the High-Tech Research Center Project, the Ministry of Education, Culture, Sports, Science and Technology (MEXT), Japan (S0801043), and from Research on Intractable Diseases, the Ministry of Health, Labour and Welfare of Japan.

References

[1] A. Serretti, P. Olgiati and D. De Ronchi, Genetics of Alzheimer's disease. A rapidly evolving field, *J Alzheimers Dis* **12** (2007), 73–92.
[2] S.F. Kingsmore, I.E. Lindquist, J. Mudge, D.D. Gessler and W.D. Beavis, Genome-wide association studies: progress and potential for drug discovery and development, *Nat Rev Drug Discov* **7** (2008), 221–230.
[3] S.D. Ginsberg, S.E. Hemby, V.M. Lee, J.H. Eberwine and J.Q. Trojanowski, Expression profile of transcripts in Alzheimer's disease tangle-bearing CA1 neurons, *Ann Neurol* **48** (2000), 77–87.
[4] V. Colangelo, J. Schurr, M.J. Ball, R.P. Pelaez, N.G. Bazan and W.J. Lukiw, Gene expression profiling of 12633 genes in Alzheimer hippocampal CA1: transcription and neurotrophic factor down-regulation and up-regulation of apoptotic and pro-inflammatory signaling, *J Neurosci Res* **70** (2002), 462–473.
[5] P. Katsel, C. Li and V. Haroutunian, Gene expression alterations in the sphingolipid metabolism pathways during progression of dementia and Alzheimer's disease: a shift toward ceramide accumulation at the earliest recognizable stages of Alzheimer's disease? *Neurochem Res* **32** (2007), 845–856.
[6] C. Williams, R. Mehrian Shai, Y. Wu, Y.H. Hsu, T. Sitzer, B. Spann, C. McCleary, Y. Mo and C.A. Miller, Transcriptome analysis of synaptoneurosomes identifies neuroplasticity genes overexpressed in incipient Alzheimer's disease, *PLoS ONE* **4** (2009), e4936.
[7] K. Oda, Y. Matsuoka, A. Funahashi and H. Kitano, A comprehensive pathway map of epidermal growth factor receptor signaling, *Mol Syst Biol* **1** (2005), 2005.0010.
[8] F. Noorbakhsh, C.M. Overall and C. Power, Deciphering complex mechanisms in neurodegenerative diseases: the advent of systems biology, *Trends Neurosci* **32** (2009), 88–100.
[9] R. Albert, H. Jeong and A.L. Barabasi, Error and attack tolerance of complex networks, *Nature* **406** (2000), 378–382.
[10] E.M. Blalock, J.W. Geddes, K.C. Chen, N.M. Porter, W.R. Markesbery and P.W. Landfield, Incipient Alzheimer's disease: microarray correlation analyses reveal major transcriptional and tumor suppressor responses, *Proc Natl Acad Sci USA* **101** (2004), 2173–2178.
[11] J.A. Miller, M.C. Oldham and D.H. Geschwind, A systems level analysis of transcriptional changes in Alzheimer's disease and normal aging, *J Neurosci* **28** (2008), 1410–1420.
[12] H. Sato, S. Ishida, K. Toda, R. Matsuda, Y. Hayashi, M. Shigetaka, M. Fukuda, Y. Wakamatsu and A. Itai, New approaches to mechanism analysis for drug discovery using DNA microarray data combined with KeyMolnet, *Curr Drug Discov Technol* **2** (2005) 89–98.
[13] D.W. Huang, B.T. Sherman and R.A. Lempicki, Systematic and integrative analysis of large gene lists using DAVID bioinformatics resources, *Nat Protoc* **4** (2009), 44–57.
[14] E.I. Boyle, S. Weng, J. Gollub, H. Jin, D. Botstein, J.M. Cherry and G. Sherlock, GO: TermFinder – open source software for accessing Gene Ontology information and finding significantly enriched Gene Ontology terms associated with a list of genes, *Bioinformatics* **20** (2004), 3710–3715.
[15] S.S. Mirra, A. Heyman, D. McKeel, S.M. Sumi, B.J. Crain, L.M. Brownlee, F.S. Vogel, J.P. Hughes, G. van Belle and L. Berg, The Consortium to Establish a Registry for Alzheimer's Disease (CERAD). Part II. Standardization of the neuropathologic assessment of Alzheimer's disease, *Neurology* **41** (1991), 479–486.
[16] H. Braak, I. Alafuzoff, T. Arzberger, H. Kretzschmar and K. Del Tredici, Staging of Alzheimer disease-associated neurofibrillary pathology using paraffin sections and immunocytochemistry, *Acta Neuropathol* **112** (2006), 389–404.
[17] T. Misawa, K. Arima, H. Mizusawa and J. Satoh, Close association of water channel AQP1 with amyloid-β deposition in Alzheimer disease brains, *Acta Neuropathol* **116** (2008), 247–260.
[18] B. Mayr and M. Montminy, Transcriptional regulation by the phosphorylation-dependent factor CREB, *Nat Rev Mol Cell Biol* **2** (2001), 599–609.
[19] B.E. Lonze and D.D. Ginty, Function and regulation of CREB family transcription factors in the nervous system, *Neuron* **35** (2002), 605–623.
[20] J. Satoh, Z. Illes, A. Peterfalvi, H. Tabunoki, C. Rozsa and T. Yamamura, Aberrant transcriptional regulatory network in T cells of multiple sclerosis, *Neurosci Lett* **422** (2007), 30–33.
[21] J. Satoh, T. Misawa, H. Tabunoki and T. Yamamura, Molecular network analysis of T-cell transcriptome suggests aberrant regulation of gene expression by NF-κB as a biomarker for relapse of multiple sclerosis, *Dis Markers* **25** (2008), 27–35.
[22] X. Zhang, D.T. Odom, S.H. Koo, M.D. Conkright, G. Canettieri, J. Best, H. Chen, R. Jenner, E. Herbolsheimer, E. Jacobsen, S. Kadam, J.R. Ecker, B. Emerson, J.B. Hogenesch, T. Unterman, R.A. Young and M. Montminy, Genome-wide analysis of cAMP-response element binding protein occupancy, phosphorylation, and target gene activation in human tissues, *Proc Natl Acad Sci USA* **102** (2005), 4459–4464.

[23] H. Viola, M. Furman, L.A. Izquierdo, M. Alonso, D.M. Barros, M.M. de Souza, I. Izquierdo and J.H. Medina, Phosphorylated cAMP response element-binding protein as a molecular marker of memory processing in rat hippocampus: effect of novelty, *J Neurosci* **20** (2000), RC112.
[24] M. Yamamoto-Sasaki, H. Ozawa, T. Saito, M. Rösler and P. Riederer, Impaired phosphorylation of cyclic AMP response element binding protein in the hippocampus of dementia of the Alzheimer type, *Brain Res* **824** (1999), 300–303.
[25] G.S. Griesbach, R.L. Sutton, D.A. Hovda, Z. Ying and F. Gomez-Pinilla, Controlled contusion injury alters molecular systems associated with cognitive performance, *J Neurosci Res* **87** (2009), 795–805.
[26] B. Gong, O.V. Vitolo, F. Trinchese, S. Liu, M. Shelanski and O. Arancio, Persistent improvement in synaptic and cognitive functions in an Alzheimer mouse model after rolipram treatment, *J Clin Invest* **114** (2004), 1624–1634.
[27] Z. Liang, F. Liu, I. Grundke-Iqbal, K. Iqbal and C.X. Gong, Down-regulation of cAMP-dependent protein kinase by over-activated calpain in Alzheimer disease brain, *J Neurochem* **103** (2007), 2462–2470.
[28] D.N. Arvanitis, A. Ducatenzeiler, J.N. Ou, E. Grodstein, S.D. Andrews, S.R. Tendulkar, A. Ribeiro-da-Silva, M. Szyf and A.C. Cuello, High intracellular concentrations of amyloid-β block nuclear translocation of phosphorylated CREB, *J Neurochem* **103** (2007), 216–228.
[29] O.V. Vitolo, A. Sant'Angelo, V. Costanzo, F. Battaglia, O. Arancio and M. Shelanski, Amyloid β-peptide inhibition of the PKA/CREB pathway and long-term potentiation: reversibility by drugs that enhance cAMP signaling, *Proc Natl Acad Sci USA* **99** (2002), 13217–13221.
[30] D. Puzzo, O. Vitolo, F. Trinchese, J.P. Jacob, A. Palmeri and O. Arancio, Amyloid-β peptide inhibits activation of the nitric oxide/cGMP/cAMP-responsive element-binding protein pathway during hippocampal synaptic plasticity, *J Neurosci* **25** (2005), 6887–6897.
[31] Q.L. Ma, M.E. Harris-White, O.J. Ubeda, M. Simmons, W. Beech, G.P. Lim, B. Teter, S.A. Frautschy and G.M. Cole, Evidence of Aβ- and transgene-dependent defects in ERK-CREB signaling in Alzheimer's models, *J Neurochem* **103** (2007), 1594–1607.
[32] Q. Li, H.F. Zhao, Z.F. Zhang, Z.G. Liu, X.R. Pei, J.B. Wang and Y. Li, Long-term green tea catechin administration prevents spatial learning and memory impairment in senescence-accelerated mouse prone-8 mice by decreasing Aβ_{1-42} oligomers and upregulating synaptic plasticity-related proteins in the hippocampus, *Neuroscience* (2009), in press, doi:10.1016/j.neuroscience.2009.07.014.
[33] F.G. De Felice, A.P. Wasilewska-Sampaio, A.C. Barbosa, F.C. Gomes, W.L. Klein and S.T. Ferreira, Cyclic AMP enhancers and Aβ oligomerization blockers as potential therapeutic agents in Alzheimer's disease, *Curr Alzheimer Res* **4** (2007), 263–271.
[34] R.A. Nixon, Autophagy, amyloidogenesis and Alzheimer disease, *J Cell Sci* **120** (2007), 4081–4091.
[35] C.V. Garat, D. Fankell, P.F. Erickson, J.E. Reusch, N.N. Bauer, I.F. McMurtry and D.J. Klemm, Platelet-derived growth factor BB induces nuclear export and proteasomal degradation of CREB via phosphatidylinositol 3-kinase/Akt signaling in pulmonary artery smooth muscle cells, *Mol Cell Biol* **26** (2006), 4934–4948.
[36] S. Costes, B. Vandewalle, C. Tourrel-Cuzin, C. Broca, N. Linck, G. Bertrand, J. Kerr-Conte, B. Portha, F. Pattou, J. Bockaert and S. Dalle, Degradation of cAMP-responsive element-binding protein by the ubiquitin-proteasome pathway contributes to glucotoxicity in beta-cells and human pancreatic islets, *Diabetes* **58** (2009) 1105–1115.
[37] K. Okamoto, S. Hirai, T. Iizuka, T. Yanagisawa and M. Watanabe, Reexamination of granulovacuolar degeneration, *Acta Neuropathol* **82** (1991), 340–345.
[38] C. Stadelmann, T.L. Deckwerth, A. Srinivasan, C. Bancher, W. Brück, K. Jellinger and H. Lassmann, Activation of caspase-3 in single neurons and autophagic granules of granulovacuolar degeneration in Alzheimer's disease. Evidence for apoptotic cell death, *Am J Pathol* **155** (1999), 1459–1466.
[39] K. Leroy, A. Boutajangout, M. Authelet, J.R. Woodgett, B.H. Anderton and J.P. Brion, The active form of glycogen synthase kinase-3β is associated with granulovacuolar degeneration in neurons in Alzheimer's disease, *Acta Neuropathol* **103** (2002), 91–99.
[40] S. Lagalwar, R.W. Berry and L.I. Binder, Relation of hippocampal phospho-SAPK/JNK granules in Alzheimer's disease and tauopathies to granulovacuolar degeneration bodies, *Acta Neuropathol* **113** (2007), 63–73.
[41] A. Thakur, X. Wang, S.L. Siedlak, G. Perry, M.A. Smith and X. Zhu, c-Jun phosphorylation in Alzheimer disease, *J Neurosci Res* **85** (2007), 1668–1673.
[42] J.J. Hoozemans, E.S. van Haastert, D.A. Nijholt, A.J. Rozemuller, P. Eikelenboom and W. Scheper, The unfolded protein response is activated in pretangle neurons in Alzheimer's disease hippocampus, *Am J Pathol* **174** (2009), 1241–1251.
[43] A. Kadokura, T. Yamazaki, S. Kakuda, K. Makioka, C.A. Lemere, Y. Fujita, M. Takatama and K. Okamoto, Phosphorylation-dependent TDP-43 antibody detects intraneuronal dot-like structures showing morphological characters of granulovacuolar degeneration, *Neurosci Lett* (2009), in press, doi:10.1016/j.neulet.2009.06.024.
[44] D.W. Dickson, H. Ksiezak-Reding, P. Davies and S.H. Yen, A monoclonal antibody that recognizes a phosphorylated epitope in Alzheimer neurofibrillary tangles, neurofilaments and tau proteins immunostains granulovacuolar degeneration, *Acta Neuropathol* **73** (1987), 254–258.
[45] W. Bondareff, C.M. Wischik, M. Novak and M. Roth, Sequestration of tau by granulovacuolar degeneration in Alzheimer's disease, *Am J Pathol* **139** (1991), 641–647.
[46] B. Boland, A. Kumar, S. Lee, F.M. Platt, J. Wegiel, W.H. Yu and R.A. Nixon, Autophagy induction and autophagosome clearance in neurons: relationship to autophagic pathology in Alzheimer's disease, *J Neurosci* **28** (2008) 6926–6937.
[47] W.Y. Ong, H.M. Lim, T.M. Lim and B. Lutz, Kainate-induced neuronal injury leads to persistent phosphorylation of cAMP response element-binding protein in glial and endothelial cells in the hippocampus, *Exp Brain Res* **131** (2000), 178–186.
[48] L.J. Cox, U. Hengst, N.G. Gurskaya, K.A. Lukyanov and S.R. Jaffrey, Intra-axonal translation and retrograde trafficking of CREB promotes neuronal survival, *Nat Cell Biol* **10** (2008) 149–159.
[49] I Granic, A.M. Dolga, I.M. Nijholt, G. van Dijk and U.L. Eisel, Inflammation and NF-κB in Alzheimer's disease and diabetes, *J Alzheimers Dis* **16** (2009), 809–821.
[50] K. Terai, A. Matsuo and P.L. McGeer, Enhancement of immunoreactivity for NF-κB in the hippocampal formation and cerebral cortex of Alzheimer's disease, *Brain Res* **735** (1996), 159–168.
[51] W.J. Lukiw, Y. Zhao and J.G. Cui, An NF-κB-sensitive micro RNA-146a-mediated inflammatory circuit in Alzheimer

disease and in stressed human brain cells, *J Biol Chem* **283** (2008), 31315–31322.
[52] D. Gezen-Ak, E. Dursun, T. Ertan, H. Hanağasi, H. Gürvit, M. Emre, E. Eker, M. Oztürk, F. Engin and S. Yilmazer, Association between vitamin D receptor gene polymorphism and Alzheimer's disease, *Tohoku J Exp Med* **212** (2007), 275–282.
[53] M.K. Sutherland, M.J. Somerville, L.K. Yoong, C. Bergeron, M.R. Haussler and D.R. McLachlan, Reduction of vitamin D hormone receptor mRNA levels in Alzheimer as compared to Huntington hippocampus: correlation with calbindin-28k mRNA levels, *Brain Res Mol Brain Res* **13** (1992), 239–250.

Biosci. Biotechnol. Biochem., 73 (6), 1443–1446, 2009

JSBA

Note

Identification of a New Pheromone-Binding Protein in the Antennae of a Geometrid Species and Preparation of Its Antibody to Analyze the Antennal Proteins of Moths Secreting Type II Sex Pheromone Components

Hayaki WATANABE, Hiroko TABUNOKI, Nami MIURA, Aya MATSUI, Ryoichi SATO, and Tetsu ANDO†

Graduate School of Bio-Applications and Systems Engineering (BASE), Tokyo University of Agriculture and Technology, Koganei, Tokyo 184-8588, Japan

Received January 13, 2009; Accepted February 17, 2009; Online Publication, June 7, 2009
[doi:10.1271/bbb.90029]

The full-length cDNA sequence of a new pheromone-binding protein (AscrPBP2) was determined from a geometrid moth, *Ascotis selenaria cretacea*, which secreted a Type II sex pheromone, and an antiserum against its recombinant protein overexpressed in *Escherichia coli* was prepared. In addition to this antiserum against AscrPBP2, antibodies against AscrPBP1 and general odorant-binding proteins of *Bombyx mori* were used in Western blotting experiments to analyze the proteins in the antennae of several lepidopteran species secreting Type II sex pheromone components.

Key words: pheromone perception; antennal protein; PCR; cDNA cloning; Geometridae in Lepidoptera

The antennae of insects include odorant-binding proteins (OBPs) to transport lipophilic odors to their receptors, which are surrounded with hemolymph. In Lepidoptera, the proteins from about 30 species have been characterized. Antennal OBPs are classified into two main groups, pheromone-binding proteins (PBPs)[1,2] for the transportation of sex pheromones and general odorant-binding proteins (GOBPs)[3] for the transportation of other odors, such as the scents of host plants. PBPs are localized mainly in the sensilla trichodea of the male antennae, and GOBPs are more abundantly expressed in the sensilla basiconica of females than in those of males.[4,5] While both proteins share some highly conserved regions, including six common cysteine residues, the former moth proteins (about 15 kDa) are further divided into three groups, Clusters A–C,[6,7] and the latter (about 17 kDa), into two groups, GOBP1 and GOBP2.

Most lepidopteran pheromones are classified into two major groups, Types I and II, according to their chemical structures.[8] Type I pheromones are composed of C_{10}–C_{18} unsaturated compounds with a terminal functional group, such as bombykol of *Bombyx mori*, and have been frequently identified from many species in various families. On the other hand, Type II pheromones identified from species in highly evolved insect groups are composed of C_{17}–C_{23} unsaturated hydrocarbons and their epoxy derivatives without a terminal functional group.[8,9] The OBPs of moths have been investigated mainly in species secreting Type I pheromones,[4,5] and information about proteins from species secreting Type II pheromones is very limited. Recently, we identified one protein (AscrPBP1) grouped in Cluster C from the antennae of the Japanese giant looper, *Ascotis selenaria cretacea*,[10] whose mating communication is mediated with (Z,Z,Z)-3,6,9-nonadecatriene and *cis*-3,4-epoxy-(Z,Z)-6,9-nonadecadiene.[11,12] This is the first identification of PBP from a species in the family of Geometridae, and no other OBPs of the insects producing Type II pheromones have been reported. Furthermore, since many lepidopteran insects produce multiple PBPs, we designed primers with reference to conserved regions in some PBPs of Clusters A and B to examine other proteins in *A. s. cretacea* antennae. In these PCR experiments, part of one gene encoding the expected length of a protein in Cluster B was amplified.[10] In order to understand the perception system of the geometrid species in detail, we determined the sequence of the full-length cDNA encoding the protein defined as AscrPBP2 in this study. Moreover, we prepared an antiserum against its recombinant protein overexpressed in *Escherichia coli* and analyzed the antennal proteins of some species secreting Type II pheromones using the antibodies against AscrPBP2 and some other OBPs. The results are presented in this report.

The sequence of the full-length cDNA of AscrPBP2 (953 bp, GenBank AB327273), shown in Fig. 1, was determined using 5′- and 3′-rapid amplification of cDNA end strategies. To determine the 5′-terminus sequence, the single-stranded cDNA was amplified with a GeneRacer 5′-primer (CGACTGGAGCACGAGGACA-CTGA), a reverse gene-specific primer for AscrPBP2 (A4), and a nested primer (A3) using a GeneRacer Kit (Invitrogen, Carlsbad, USA). Single-stranded cDNA for 3′-RACE was prepared from antennal mRNA (100 males) with an oligo(dT)-M13 adaptor primer (AGC-GGATAACAATTTCACACAGGAAAC) and ReverTra Ace, and amplified with the forward gene-specific primers for AscrPBP2 (S4) and nested (S3). The cDNA included an open-reading frame of 489 nucleotides encoding 162 amino acids, using ATG (49–51) as an

† To whom correspondence should be addressed. Tel/Fax: +81-42-388-7278; E-mail: antetsu@cc.tuat.ac.jp

```
GAAAAACAGCTGATCCTTCTGTGGCTGGTCTCGTAGATACAGAACAAAATGAGGACTAATAAAGTAGTTTTGATACTCTTAATGAGTATG  90
                                               M  R  T  N  K  V  V  L  I  L  L  M  S  M  14
              GSF2
ATAGCCATAGTGACACCATCGCAAGATGTAATGAAGACTTTGACCATCAACTTCGGAAAACCTATGGAAATTTGCAAGAAAGAGCTGGAT 180
 I  A  I  V  T  P  S  Q  D  V  M  K  T  L  T  I  N  F  G  K  P  M  E  I  C  K  K  E  L  D  44
                                                                            *
                                        DF3                     S3                     A3
TTACCTGAGGCAGTGACTAAAGAGTTCCTAAACTTTTGGCGAGATGGCTACGAGGTGACCAACCGCCTGACTGGCTGTGCCATCATGTGC 270
 L  P  E  A  V  T  K  E  F  L  N  F  W  R  D  G  Y  E  V  T  N  R  L  T  G  C  A  I  M  C  74
                                                                               *           *
             S4                A4                          DR1
ATTTCGGAGAAGCTGGAGCTGCTCGACGAGGGATATAAACTCCATCATGGAAACGCAAAGGACTTCGCTATGAAACATGGAGCTGACGCC 360
 I  S  E  K  L  E  L  L  D  E  G  Y  K  L  H  H  G  N  A  K  D  F  A  M  K  H  G  A  D  A 104

GGCATGGCGCAGCAGCTGGTGGACATCATCCACGGCTGCAACGAGAGCACCCCAGACAACACAGACCATTGCCTCAAGACAGTCGCCGTG 450
 G  M  A  Q  Q  L  V  D  I  I  H  G  C  N  E  S  T  P  D  N  T  D  H  C  L  K  T  V  A  V 134
                                     *                                      *
                                                                                 GSR2
GCCATGTGCTTCAAGCACAAGATTCACGAGCTGGACTGGGCTCCAAACGCTGACCTCATCATTGCTGAGGTCCTTGCTGAAGTATAAACC 540
 A  M  C  F  K  H  K  I  H  E  L  D  W  A  P  N  A  D  L  I  I  A  E  V  L  A  E  V  x     162
       *
CGTCCTTGCTGAAGTGTAACCTCCTTCCTCCACCATTCGACTTCCTGGAAATTGCTTAAAAACCACTATCGCTCTGACGACAAAATTCTC 630
CTGCAAGTGCTTTTATGCAAAGTGAACGTCTAACTTTGCGAGTGTTGTAATTTCTATCACCACGGCTTTCTCATCGTGAACGGACGAAGT 720
TCTTCGGCGGAACTAAATGAAGTGGAAGACGGTCAGCAGTAGTGATTTTCAAAGCGTGTTCCATCAGCGACATGGGGGTCCTAGAAATGT 810
CCCAAACTGACCTAGCTAAGAAGATGGAATCTTGATTTTGTGTGCTTGCTCGCCTTTTTCAGCTGTCGATTTTATTTTACTATATTTTAA 900
TGGTTATTAATAAATGTTTGATGAGTATGATCTGAAAAAAAAAAAAAAAAAAA 953
```

Fig. 1. Nucleotide and Deduced Amino Acid Sequences of AscrPBP2 cDNA (GenBank AB327273).

The suggested start codon ATG and the stop codon TAA are indicated in boxes. A putative signal peptide at the *N*-terminus is shown by a dotted underline, and six cysteine residues are marked with asterisks. The positions of the primers used in PCR amplification are indicated by arrows, as follows: degenerate primers (DF3 and DR1), gene-specific primers for 3′ RACE [S3 and S4 (nested)], 5′ RACE [A3 (nested) and A4], and RT-PCR or expression in *E. coli* (GSF2 and GSR2).

initiation codon and TAA (535–537) as a termination codon. In addition, the first methionine and a putative signal sequence of 20 amino acids (49–109) were predicted by NetStart (http://www.cbs.dtu.dk/services/NetStart/) and SignalP (http://www.cbs.dtu.dk/services/SignalP/), respectively. The 3′-terminus sequence included a putative polyadenylation signal sequence, AATAAA, with the poly (A) tail beginning at the 909 position.

The mature AscrPBP2 protein had a deduced molecular mass of 15,902 Da and a pI of 5.02. It had an acidic isoelectric point and conservative six cysteine residues (Cys^{19}, Cys^{50}, Cys^{54}, Cys^{97}, Cys^{108}, and Cys^{117}), similarly to PBPs identified from other lepidopteran species. Phylogenetic analysis of the amino acid sequences of AscrPBP2 and other known PBPs confirmed that this protein was to be classified into Cluster B, as shown in Fig. 2. While the similarity between AscrPBP1 and AscrPBP2 is 40%, that between AscrPBP2 and other proteins in Cluster B is about 60%. A preliminary binding experiment on AscrPBP2, which was carried out in a manner similar to that for AscrPBP1,[10] indicated its binding of the pheromone components of *A. s. cretacea* (data not shown). Because both AscrPBP1 and AscrPBP2, with an ability to bind Type II pheromone components, are defined as proteins in the known clusters, it appears that the differences among the clusters are not caused by structural differences in the bound pheromones. It would be interesting to know whether each cluster covers a specific function.

The specific distribution of Ascr-PBP2 in antennae was confirmed by RT-PCR analysis, which was performed with primers, GSF2 and GSR2, and cDNAs prepared from various tissues of *A. s. cretacea* (Fig. 3A). Furthermore, an antiserum against a recombinant protein of AscrPBP2 was prepared in a manner similar to that of AscrPBP1.[10] The coding region for the

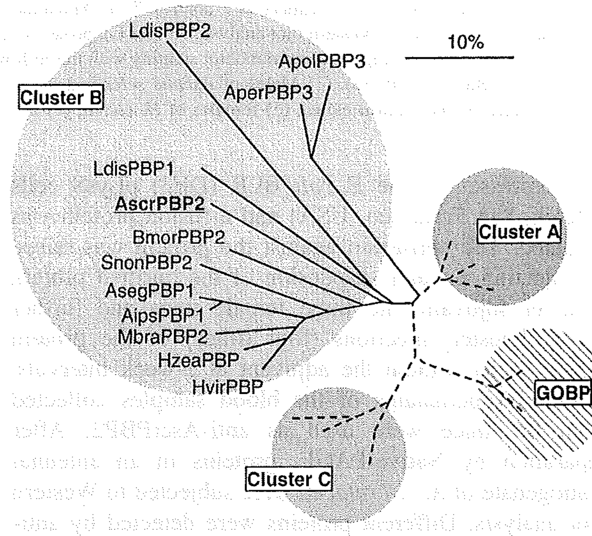

Fig. 2. Phylogenetic Tree of PBPs in Cluster B Identified from Lepidopteran Insects (GenBank Accession Numbers).

Lineage analysis was based on their amino acids using CLUSTALW by the neighbor-joining method (http://www.ddbj.nig.ac.jp/search/clustalw-j.html), and the phylogenetic tree was visualized by TreeView. Branch lengths are proportional to the percentage sequence difference: scale bar, 10% difference. *Agrotis ipsilon* (AipsPBP1: AY301985), *A. segetum* (AsegPBP1: AF134253), *Antheraea pernyi* (AperPBP3: AJ277265), *A. polyphemus* (ApolPBP3: AJ277267), *Ascotis selenaria cretacea* (AscrPBP2: AB327273, this work), *Bombyx mori* (BmorPBP2: AM403100), *Helicoverpa zea* (HzeaPBP: AF090191), *Heliothis virescens* (HvirPBP: X96861), *Lymantria dispar* (LdisPBP1: AF007867, LdisPBP2: AF007868), *Mamestra brassicae* (MbraPBP2: AF051142), and *Sesamia nonagrioides* (SnonPBP2: AY485220).

putative mature protein of AscrPBP2 was amplified by PCR using specific primers (GSF2 and GSR2, Fig. 1) encoding BamHI (Takara Bio, Ohtus, Japan) and XhoI (Takara Bio) recognition sites. Each PCR product was cloned in the GST fusion protein expression vector pGX-4T-3 (GE Healthcare UK, Buckinghamshire, UK)

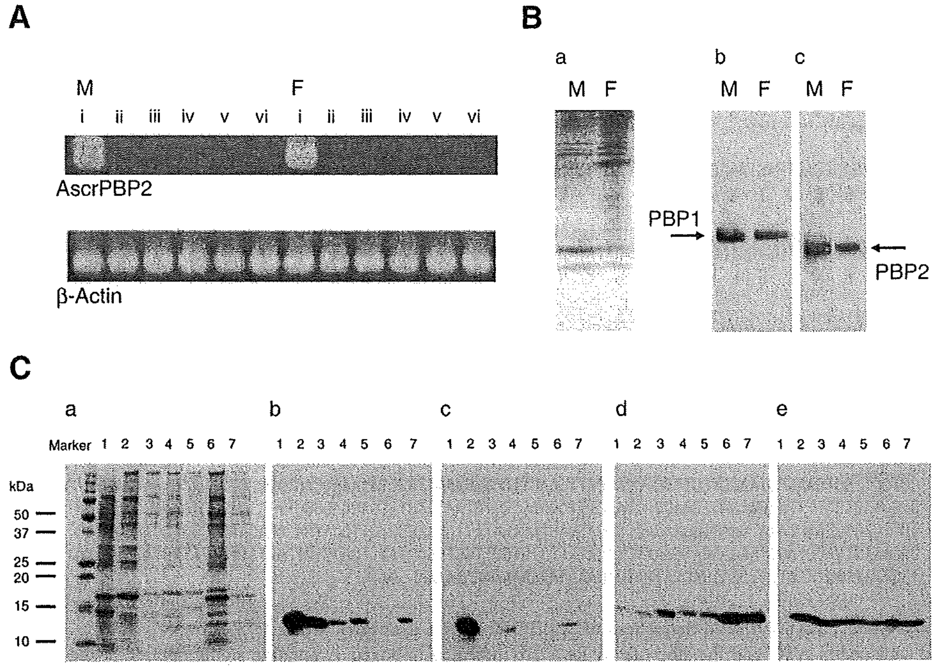

Fig. 3. Transcript and Protein Levels of Odorant-Binding Proteins; RT-PCR Analysis for Tissue Distribution of AscrPBP2 in Males and Females of *Ascotis selenaria cretacea* (A), and Western Blot Analyses of Antennal Proteins of *A. s. cretacea* with Two Antibodies after Native PAGE (B) and Five Moth Species with Four Antibodies after SDS PAGE (C).

In gene expression of AscrPBP2 (A), RT-PCR was performed with specific primers and cDNA prepared from the tissues. β-Actin cDNA was also amplified with β-actin primers as a control.[10] (i) Antennae, (ii) heads without antennae, (iii) thoraxes, (iv) abdomens, (v) legs, and (vi) abdominal tips. In the Western blot analyses (B and C), proteins in the homogenates of male and female antennae (100 each) were visualized by Coomassie blue staining (a) or immunoblot staining with the following antibodies: anti-AscrPBP1 (b), anti-AscrPBP2 (c), anti-BmorGOBP1 (d), and anti-BmorGOBP2 (e). (1) Males of *Ascotis selenaria cretacea*, (2) males of *Hemerophila atrilineata*, (3) males of *Syntomoides imaon*, (4) males of *Hyphantria cunea*, (5) females of *H. cunea*, (6) males of *Bombyx mori*, and (7) females of *B. mori*.

and expressed in the *E. coli* BLR (DE3) pLysS cells (Merck, San Francisco, USA) and a fusion protein was obtained. The antiserum against the protein was raised by injecting a water suspension of the purified protein with an adjuvant into three female mice and further giving booster injections (four times) of the protein (15 µg each) without the adjuvant at 1-week intervals. Cultured supernatants of the blood samples collected from the mice were used as anti-AscrPBP2. After separation by Native-PAGE, proteins in an antennal homogenate of *A. s. cretacea* were subjected to Western blot analysis. Different proteins were detected by anti-AscrPBP1 and anti-AscrPBP2 (Fig. 3B), suggesting that these antibodies were not cross-reactive. This analysis also revealed that AscrPBP2 is protein X, which was detected to be more abundant than AscrPBP1 in our previous experiment.[10]

In addition to anti-AscrPBPs, previously prepared antibodies for GOBPs of *B. mori* (anti-BmorGOBP1 and anti-BomrGOBP2)[10] were used in Western blotting experiments to analyze the proteins in the antennae of *B. mori*, *A. s. cretacea*, and the following three species with Type II sex pheromones: mulberry looper (*Hemerophila atrilineata*, Geometridae),[13,14] fall webworm moth (*Hyphantria cunea*, Arctiidae),[15] and wasp moth (*Syntomoides imaon*, Arctiidae).[16] Figure 3C shows the proteins visualized by immunoblot staining with the antibodies after SDS–PAGE. This analysis indicated that both anti-BmorGOBP1 and anti-BomrGOBP2 were reactive to antennal proteins not only of *B. mori* but also of all the other species. Since these antibodies are not cross-reactive against each other,[10] it would appear that the two GOBPs occur in the antennae of species secreting Type II pheromones as often as they do in those of species secreting Type I pheromones. On the other hand, all male antennae included the protein detected by anti-AscrPBP1, but anti-AscrPBP2 detected nothing in the antennae of *H. atrilineata* and *H. cunea*. Anti-AscrPBP2 interestingly stained a protein in the male antennae of *B. mori*, which included PBP in Cluster B.[7] Since the specific recognition regions of the polyclonal antibodies remain unidentified, it is difficult to conclude the details of PBPs included in the antennae examined. The specificities of these antiserums against the PBPs of many other insects ought to be examined. The experiment with anti-AscrPBP1, however, indicated that the reactivity of anti-AscrPBP1 might be wide among the insect species examined, and that each species might have PBP in Cluster C. The experiment with anti-AscrPBP2 suggests its narrow reactivity as one possibility. If the antibody has wide reactivity as another possibility, it can be deduced that *H. atrilineata* and *H. cunea* express no proteins in Cluster B in their antennae. In addition, molecular studies are necessary to investigate the PBPs of many species secreting Type II pheromones.

While pheromone receptors strictly recognize the structures of pheromone components, the binding specificity of PBP is not high, as indicated by our previous experiment with AscrPBP1,[10] suggesting a supporting role in the perception of a species-specific pheromone by each species. Recent research with fruit flies expressing receptor and PBP genes of *B. mori*, however, indicates that stimulation of a receptor is effectively accomplished by direct interaction between the receptor and PBP.[17] On the basis of our identification of PBPs in *A. s. cretacea* antennae, the entire perception system of Type II pheromones can be accurately understood.

References

1) Vogt RG and Riddiford LM, *Nature*, **293**, 161–163 (1981).
2) Prestwich GD, *Bioorg. Med. Chem.*, **4**, 505–513 (1996).
3) Bree H, Krieger J, and Raming K, *Insect Biochem.*, **20**, 735–740 (1990).
4) Vogt RG, "Insect Pheromone Biochemistry and Molecular Biology," eds. Blomquist GJ and Vogt RG, Elsevier, London, pp. 391–445 (2003).
5) Leal WS, *Top. Curr. Chem.*, **240**, 1–36 (2005).
6) Abraham D, Löfstedt C, and Picimbon JF, *Insect Biochem. Mol. Biol.*, **35**, 1100–1111 (2005).
7) Forstner M, Gohl T, Breer H, and Krieger J, *Invert. Neurosci.*, **6**, 177–187 (2006).
8) Ando T, Inomata S, and Yamamoto M, *Top. Curr. Chem.*, **239**, 51–96 (2004).
9) Millar JG, *Annu. Rev. Entomol.*, **45**, 575–604 (2000).
10) Watanabe H, Tabunoki H, Miura N, Sato R, and Ando T, *Invert. Neurosci.*, **7**, 109–118 (2007).
11) Ando T, Ohtani K, Yamamoto M, Miyamoto T, Qin XR, and Witjaksono, *J. Chem. Ecol.*, **23**, 2413–2423 (1997).
12) Witjaksono, Ohtani K, Yamamoto M, Miyamoto T, and Ando T, *J. Chem. Ecol.*, **25**, 1633–1642 (1999).
13) Tan Z-X, Gries R, Gries G, Lin G-Q, Pu G-Q, Slessor KN, and Li J-X, *J. Chem. Ecol.*, **22**, 2263–2271 (1996).
14) Pu G-Q, Yamamoto M, Takeuchi Y, Yamazawa H, and Ando T, *J. Chem. Ecol.*, **25**, 1151–1162 (1999).
15) Tóth M, Buser HR, Peña A, Arn H, Mori K, Takeuchi T, Nikolaeva LN, and Kovalev BG, *Tetrahedron Lett.*, **30**, 3405–3408 (1989).
16) Matsuoka K, Yamamoto M, Yamakawa R, Muramatsu M, Naka H, Kondo Y, and Ando T, *J. Chem. Ecol.*, **34**, 1437–1445 (2008).
17) Syed Z, Ishida Y, Taylor K, Kimbrell DA, and Leal WS, *Proc. Natl. Acad. Sci. USA*, **103**, 16538–16543 (2006).

NEUROPATHOLOGY

Neuropathology 2010; **30**, 7–14 doi:10.1111/j.1440-1789.2009.01035.x

Original Article

Protein microarray analysis identifies cyclic nucleotide phosphodiesterase as an interactor of Nogo-A

Kenta Sumiyoshi,[1] Shinya Obayashi,[1] Hiroko Tabunoki,[1] Kunimasa Arima[2] and Jun-ichi Satoh[1]

[1]Department of Bioinformatics and Molecular Neuropathology, Meiji Pharmaceutical University, and [2]Department of Psychiatry, National Center Hospital, NCNP, Tokyo, Japan

Nogo-A, a neurite outgrowth inhibitor, is expressed exclusively on oligodendrocytes and neurons in the CNS. The central domain of Amino-Nogo spanning amino acids 567–748 in the human Nogo-A designated NIG, mediates persistent inhibition of axonal outgrowth and induces growth cone collapse by signaling through an as yet unidentified NIG receptor. We identified 82 NIG-interacting proteins by screening a high-density human protein microarray composed of 5000 proteins with a recombinant NIG protein as a probe. Following an intensive database search, we selected 12 neuron/oligodendrocyte-associated NIG interactors. Among them, we verified the molecular interaction of NIG with 2′, 3′-cyclic nucleotide 3′-phosphodiesterase (CNP), a cell type-specific marker of oligodendrocytes, by immunoprecipitation and cell imaging analysis. Although CNP located chiefly in the cytoplasm of oligodendrocytes might not serve as a cell-surface NIG receptor, it could act as a conformational stabilizer for the intrinsically unstructured large segment of Amino-Nogo.

Key words: CNP, NIG, Nogo-A, protein microarray, protein-protein interaction.

INTRODUCTION

Nogo is a family of myelin-associated inhibitors for axonal regeneration in the CNS.[1] It consists of three isoforms named A, B and C, all of which share a C-terminal 66 amino acid segment named Nogo-66. Nogo-A, the longest isoform with the strongest activity of neurite outgrowth inhibition, is expressed exclusively in myelin sheaths and oligodendrocytes on the cell surface and in the endoplasmic reticulum (ER), in addition to a subpopulation of neurons in the adult CNS. Nogo-A also plays a key role in maturation of oligodendrocytes *in vivo*.[2] Nogo-B is ubiquitously distributed both inside and outside the CNS, while Nogo-C, the shortest isoform, is enriched in skeletal muscle. Nogo-A has at least two discrete domains that exhibit neuronal growth-inhibitory activities.[3] One is located in the Nogo-A-specific C-terminal segment of Amino-Nogo, and the other is Nogo-66. The N-terminal segment of Amino-Nogo, shared between Nogo-A and Nogo-B, plays a role in vascular remodeling. Nogo-66, along with oligodendrocyte-myelin glycoprotein (OMgp) and myelin-associated glycoprotein (MAG), transduces inhibitory signals via a molecular complex composed of the Nogo receptor (NgR), Lingo-1, and p75^{NTR} or Troy by activating RhoA that mediates actin depolymerization responsible for the collapse of growth cones on regenerating axons.[1]

The Nogo-A-specific C-terminal segment of Amino-Nogo, being conformationally unfolded,[4,5] mediates persistent inhibition of axonal outgrowth and induces growth cone collapse via the NgR-independent mechanism.[6] The central region of this segment spanning amino acids 567–748 in the human Nogo-A designated NIG, is pivotal for this activity.[3] Because the NIG domain exists only in Nogo-A, it provides an explanation for Nogo-A acting as the most potent inhibitor of axonal growth among three Nogo isoforms. Importantly, treatment with the antibody raised against the Nogo-A-specific domain enhances sprouting of corticospinal axons and promotes functional recovery following spinal cord injury in adult primates.[7] A previous study showed that the predominant proteins that

Correspondence: Jun-ichi Satoh, MD, Department of Bioinformatics and Molecular Neuropathology, Meiji Pharmaceutical University, 2-522-1 Noshio, Kiyose, Tokyo 204-8588, Japan. Email: satoj@my-pharm.ac.jp

Received 18 March 2009; Revised 13 April 2009; Accepted 14 April 2009; published online 7 June 2009.

interact with Nogo-A are Nogo-B and Nogo-C.[8] Although Amino-Nogo interacts with α5 and αv integrins,[9] the NIG-specific receptor remains to be characterized.

Recently, protein microarray technology has been established for rapid and systematic screening of protein-protein interactions in a high-throughput fashion.[10] The protein microarray is a chip on which thousands of functional proteins are immobilized. By reacting the array with the specific protein as a probe, it enables us to efficiently identify the target protein on chip as a binding partner. Protein microarray has a wide range of applications, including characterization of antibody specificity and autoantibody repertoire, and identification of novel biomarkers and molecular targets associated with disease type, stage and progression.[10] In the present study, we attempted to characterize a comprehensive profile of NIG-interacting proteins, which might include a candidate for NIG receptors, by using the high-density human protein microarray.

MATERIALS AND METHODS

Protein microarray analysis

We utilized ProtoArray v3.0 (Invitrogen, Carlsbad, CA, USA) that contains 5000 recombinant glutathione S-transferase (GST)-tagged human proteins expressed by the baculovirus expression system. They are purified to ensure the preservation of native structure, post-translational modifications, and proper functionality, as described previously.[11,12] The target proteins cover a wide range of biologically important proteins, and the complete list is shown in Table S1 online. The proteins are spotted on the glass slide in an arrangement of 4 × 12 subarrays equally spaced in vertical and horizontal directions. Because target proteins on the array protrude from the surface via N-terminal GST serving as a spacer, the probe is spatially accessible to all parts of them. Each subarray includes 20 × 20 spots, composed of 76 positive and negative control spots, 222 human target proteins, and 102 blanks and empty spots.

To prepare the probe for microarray analysis, the gene encoding the human NIG domain (NM_020532) was amplified by PCR with the primer set of 5′actggtacaaagat tgcttatgaa3′ and 5′aaataagtcaactggttcagaatc3′. It is worthy to note that the amino acid sequence of human NIG shows 82% and 80% identity to the rat or mouse ortholog, respectively. The PCR product was first cloned into the vector pSecTag/FRT/V5-His-TOPO (Invitrogen). Then, the gene segment coding for V5-tagged NIG was transferred into the vector pTrcHis-TOPO (Invitrogen). The V5-tagged NIG protein was expressed in *E. coli* and purified from the lysate by passing through the histidine-tagged proteins (HIS)-select spin column (Sigma, St. Louis, MO, USA), as described previously.[11,12] The purity and specificity of the probe were verified by silver stain and Western blot with mouse monoclonal anti-V5 antibody (Invitrogen) and sheep polyclonal anti-human NIG antibody (AF3515; R&D Systems, Minneapolis, MN, USA).

To block non-specific binding, the array was incubated at 4°C for 1 h with the phosphate-buffered saline supplemented with Tween 20 (PBST) blocking buffer, composed of 1% bovine serum albumin (BSA) and 0.1% Tween 20 in phosphate-buffered saline (PBS). Then, the array was incubated at 4°C for 90 min with the probe described above at a concentration of 100 μg/mL in the probing buffer, according to the methods described previously.[11,12] The array was then incubated at 4°C for 30 min with Alexa Fluor 647-conjugated mouse monoclonal anti-V5 antibody (Invitrogen). After washing, it was scanned by the GenePix 4200A scanner (Axon Instruments, Union City, CA, USA) at a wavelength of 635 nm. The data were analyzed by using the ProtoArray Prospector software v4.0 (Invitrogen), following acquisition of the microarray lot-specific information that compensates inter-lot variations among arrays in protein concentrations identified by the post-printing quality control. The spots showing the background-subtracted signal intensity value greater than the median plus three standard deviations of all the fluorescence intensities were considered as having significant interactions. The Z-score was calculated as the background-subtracted signal intensity value of the target protein minus the average of the background-subtracted signal intensity value from the negative control distribution, divided by the standard deviation of the negative control distribution. The cut-off value of Z-score was set as 3, as described previously.[11,12]

Immunoprecipitation and Western blot analysis

The coimmunoprecipitation analysis was performed according to the methods described previously.[11,12] In brief, the protein extract was prepared from the cells and tissues solubilized in mammalian protein extraction reagent (M-PER) protein extraction buffer (Pierce, Rockford, IL, USA). After preclearance, it was processed for immunoprecipitation with rabbit polyclonal anti-Nogo-A antibody (H-300; Santa Cruz Biotechnology, Santa Cruz, CA, USA) or rabbit polyclonal anti-2′, 3′-cyclic nucleotide 3′-phosphodiesterase (CNP) antibody (M-300; Santa Cruz Biotechnology). The precipitates were then processed for Western blot with anti-NIG antibody (AF3515) or mouse monoclonal anti-CNP antibody (11-5B; Sigma). The negative control included normal rabbit IgG instead of specific antibodies during the immunoprecipitation process. The specific reaction was visualized by using a chemiluminescence substrate (Pierce).

To specify the CNP-interacting domain of Nogo-A, the protein extract of HEK293 cells, in which the transgenes encoding NIG and CNP were coexpressed, was processed for coimmunoprecipition analysis. To achieve this, the NIG gene or the full-length CNP gene was amplified by PCR, and cloned into the expression vector p3XFLAG-CMV7.1 (Sigma) or pCMV-Myc (Clontech, Mountain View, CA, USA) to express a fusion protein with an N-terminal Flag or Myc tag, respectively. After cotransfection of the vectors in HEK293 cells, the protein extract was processed for immunoprecipitation with mouse monoclonal anti-Flag M2 affinity gel (Sigma) or rabbit polyclonal anti-Myc-conjugated agarose (Sigma). This was followed by Western blot with rabbit polyclonal anti-Myc antibody (Sigma) and mouse monoclonal anti-FLAG M2 antibody (Sigma).

Cell imaging, immunocytochemistry and immunohistochemistry

To determine coexpression of NIG and CNP in neural cell cultures, the NIG gene or the full-length CNP was cloned into the expression vector pDsRed-Express-C1 (Clontech) or pFN2A CMV Flexi (Promega, Madison, WI, USA) to express a fusion protein with an N-terminal DsRed or Halo tag, respectively. They were cotransfected in SK-N-SH neuroblastoma cells. At 24–48 h after transfection, the cells were exposed to Oregon Green (Promega), a fluorochrome specifically bound to the Halo tag protein. In some experiments, primary cultures established from the brain of newborn Institute of Cancer Research (ICR) mice were processed for double-immunolabeling with anti-NIG antibody (AF3515) and anti-CNP antibody (11-5B), followed by labeling with Alexa Fluor 568-conjugated anti-sheep IgG (Invitrogen) and Alexa Fluor 488-conjugated anti-mouse IgG (Invitrogen). Subsequently, the cells were fixed briefly in 4% paraformaldehyde, exposed to 4′, 6′-diamidino-2-phenylindole (DAPI; Invitrogen), mounted on slides with glycerol-polyvinyl alcohol, and examined on the Olympus BX51 universal microscope.

For double-labeling immunohistochemistry, deparaffinated tissue sections were heated in 10 mmol/L citrate sodium buffer, pH 6.0 by autoclave for 30 s at 125°C in a temperature-controlled pressure chamber (Dako, Tokyo, Japan). They were incubated with PBS containing 10% normal goat serum for 15 min at room temperature (RT) to block non-specific staining. Then, tissue sections were stained at RT overnight with anti-CNP antibody (11-5B), followed by incubation with alkaline phosphatase (AP)-conjugated anti-mouse IgG (Nichirei, Tokyo, Japan), and colorized with New Fuchsin substrate. After inactivation of the antibody by autoclaving the sections at 125°C for 30 s in 10 mM citrate sodium buffer, pH 6.0, the tissue sections were treated for 15 min with 3% hydrogen peroxide-containing distilled water to block the endogenous peroxidase activity. Then, they were relabeled with anti-Nogo-A antibody (H-300) or anti-NIG antibody (AF-3515), followed by incubation with horseradish peroxidase (HRP)-conjugated secondary antibodies, and colorized with DAB substrate and a counterstain with hematoxylin. For negative controls, the step of incubation with primary antibodies was omitted.

RESULTS

Protein microarray-identified 82 NIG interactors

For protein microarray analysis, we prepared a highly purified V5-tagged NIG probe showing a single 45-kDa band in a 12% SDS-PAGE gel (Fig. 1a, lanes 1–3). By screening the protein microarray with this probe, we identified 82 proteins as those showing significant interaction with NIG among 5000 proteins on the array. They are listed in Table S2 online. Because Nogo-A is located not only on the plasma membrane of oligodendrocytes, but also in the ER where the NIG domain is exposed to the cytosol,[13] it is not surprising that many extramembrane proteins are listed in NIG-interacting partners.

Selection of CNP as the most probable NIG interactor candidate

First, for 82 NIG interactors, we investigated the EST profile on UniGene (http://www.ncbi.nlm.nih.gov/UniGene), the protein expression profile on Human Protein Reference Database (HPRD; http://www.hprd.org), and the mRNA expression profile of mouse orthologs in the brain on the Allen Brain Atlas (ABA) database (http://www.brain-map.org), a high-throughput *in situ* hybridization atlas of gene expression pattern in the adult mouse brain.[14] The database search suggested that the great majority of 82 NIG interactors represent non-neural proteins, suggesting the promiscuous binding of most NIG interactors in a non-physiological setting on the array. Therefore, we focused exclusively on the proteins whose expression in the CNS is supported by the expression profiling on UniGene, HRPD and ABA databases. Subsequently, we identified the proteins highly relevant to the biological function of Nogo-A by searching on PubMed by importing brain, neuron, neurite, axon, myelin, or oligodendrocyte as search terms. Following intensive search, we retrieved 12 neuron/oligodendrocyte-associated NIG interactors that were hit by any of these key words (Table 1). Among them, we finally found that only CNP (the spots in Fig. 1b), a cell type-specific marker for oligodendrocytes, has a physiological relevance to axon, myelin and oligodendrocytes (see the details in the Discussion section).

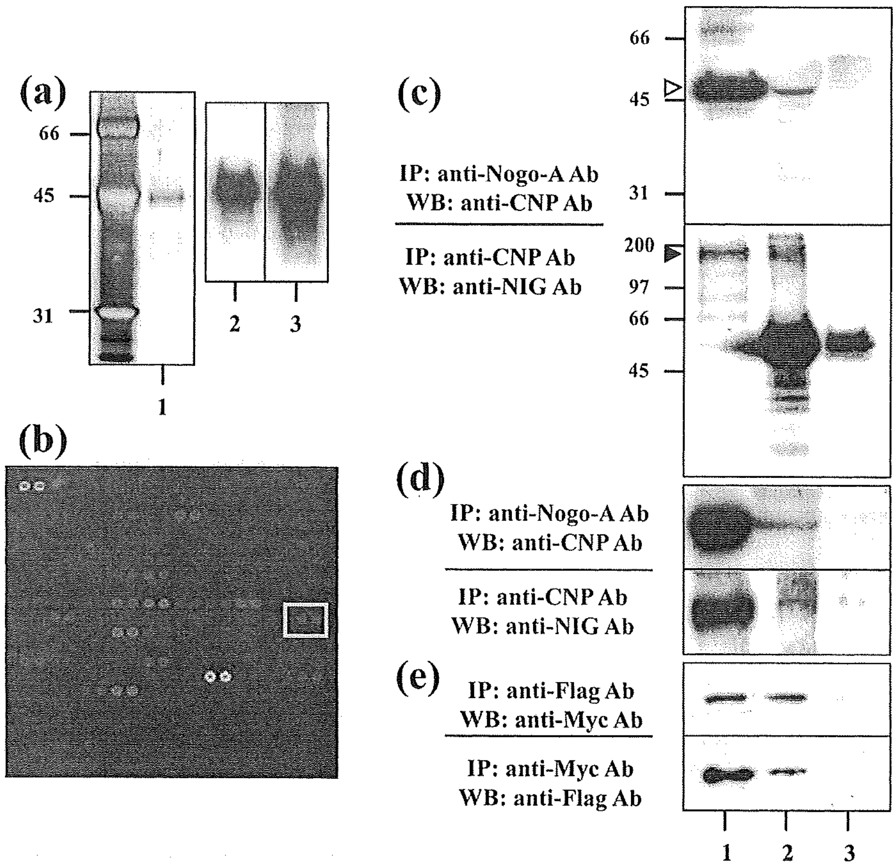

Fig. 1 Protein microarray and immunoprecipitation analysis. (a) The V5-tagged NIG-specific probe utilized for microarray analysis. The probe (0.3 μg each lane) was separated by a 12% SDS-PAGE gel. The silver stain of the gel with the position of molecular weight markers (lane 1). The blot was labeled with anti-V5 antibody (lane 2) and anti-human NIG antibody (lane 3). (b) Anti-2′, 3′-cyclic nucleotide 3′-phosphodiesterase (CNP) identified as a NIG interactor on the array. The protein microarray containing duplicate spots of 5000 proteins is composed of 4 × 12 subarrays. Each subarray includes 20 × 20 spots, composed of 76 control spots, including 14 positive and 62 negative control spots, 222 human target proteins, and 102 blanks and empty spots. The subarray No. 20 is shown. The spots positioned at row 10, columns 19, 20 indicated by an enclosed yellow line represent CNP. (c–e) Immunoprecipitation (IP) and Western blot (WB). Anti-Nogo-A antibody pulled down the endogenous CNP (open arrow, 47-kDa), while anti-CNP antibody precipitated the endogenous full-length Nogo-A (filled arrow, 190-kDa) from (c) the human brain homogenate, and from (d) the rat C6 glioma cell lysate. (e) The NIG gene and the CNP gene were cloned into the expression vectors to express a fusion protein with a Flag or Myc tag, respectively. They were cotransfected in HEK293 cells, and the lysate was processed for immunoprecipitation analysis with anti-Flag antibody and anti-Myc antibody. The lanes (1–3) of (c–e) represent (1) input control, (2) IP with the target-specific antibody, and (c) IP with normal mouse or rabbit IgG.

Validation of the interaction between NIG and CNP

Next, we verified the molecular interaction between Nogo-A and CNP by coimmunoprecipitation analysis. Anti-Nogo-A antibody (H-300) pulled down the endogenous CNP (47-kDa) labeled with anti-CNP antibody, while anti-CNP antibody (M-300) precipitated the full-length Nogo-A (190-kDa) labeled with anti-NIG antibody from both the human brain homogenate and the lysate of rat C6 glioma cells (Fig. 1c,d, upper and lower panels, lane 2). In contrast, the inclusion of normal IgG instead of H-300 or M-300 antibody recovered neither CNP nor Nogo-A (Fig. 1c,d, upper and lower panels, lane 3), supporting the specificity of the interaction. These results indicate that the endogenous Nogo-A interacts with the endogenous CNP *in vitro* and *in vivo*.

To specify the CNP-interacting domain of Nogo-A, the NIG gene or the CNP gene was cloned into the two different expression vectors to express a fusion protein with an N-terminal Flag or Myc tag. After cotransfection of the vectors in HEK293 cells, the protein extract was processed for immunoprecipitation with mouse monoclonal anti-Flag M2 affinity gel, rabbit polyclonal anti-Myc-conjugated agarose, or the same amount of normal mouse or rabbit IgG-conjugated agarose, followed by Western blot with rabbit polyclonal anti-Myc antibody and mouse monoclonal anti-FLAG M2 antibody. The reciprocal coimmunoprecipitation analysis verified the interaction of the NIG domain of Nogo-A and CNP (Fig. 1e, upper and lower panels, lane 2). These results indicate that the NIG domain of Nogo-A on its own interacts with CNP, but do not exclude the possibility that the domain located outside NIG is also bound to CNP.

To determine subcellular colocation of NIG and CNP, the NIG gene or the CNP gene was cloned into the two different expression vectors to express a fusion protein with an N-terminal DsRed or Halo tag. When cotransfected in SK-N-SH neuroblastoma cells, NIG was expressed not only on the plasma membrane but also in the cytoplasm, and at low amounts in the nucleus. DsRed-tagged NIG and Oregon Green-labeled CNP were coexpressed chiefly in the cytoplasm (Fig. 2, panels a–c). Furthermore, coexpression of NIG and CNP was identified

Table 1 Twelve neuron/oligodendrocyte-associated NIG interactors

No.	Gene symbol	Gene name	Z-score	Putative function
1	RPL31	Ribosomal protein L31	7.22386	A ribosomal protein that constitutes a component of the 60S subunit
2	CIRBP	Cold inducible RNA binding protein	6.76639	A cold-shock protein that plays a role in cold-induced suppression of cell proliferation
3	PLK3	Polo-like kinase 3 (Drosophila)	6.51572	A serine/threonine kinase that plays a role in regulation of cell cycle progression
4	MARK4	MAP/microtubule affinity-regulating kinase 4	5.45038	A serine/threonine kinase involved in microtubule organization in neuronal cells
5	RPL30	Ribosomal protein L30	4.82371	A ribosomal protein that constitutes a component of the 60S subunit
6	CNP	2′,3′-cyclic nucleotide 3′ phosphodiesterase	4.71717	A membrane-bound enzyme located in the CNS myelin
7	FGF13	Fibroblast growth factor 13	4.35684	A member of the fibroblast growth factor family
8	ZNF192	Zinc finger protein 192	4.09363	A transcription factor of unknown function
9	NHP2	Nucleolar protein family A, member 2 (H/ACA small nucleolar RNPs)	4.04663	A member of the H/ACA snoRNPs gene family
10	ATP5O	ATP synthase, H+ transporting, mitochondrial F1 complex, O subunit (oligomycin sensitivity conferring protein)	3.25389	A component of the F-type ATPase located in the mitochondrial matrix
11	ODC1	Ornithine decarboxylase 1	3.06902	The rate-limiting enzyme of the polyamine biosynthesis pathway that catalyzes ornithine to putrescine
12	EIF2C1	Eukaryotic translation initiation factor 2C, 1	3.00322	A member of the Argonaute family that plays a role in RNA interference

Among 82 NIG interactor candidates (Table S2), 12 were categorized as neuron/oligodendrocyte-associated NIG interactors by database search on UniGene, HPRD, and Allen Brain Atlas, and by the PubMed search with brain, neuron, neurite, axon, myelin, or oligodendrocyte as search terms. Among them, we found that only CNP (No. 6) has a physiological relevance to axon, myelin and oligodendrocytes.

both in the cytoplasm and on the cell surface of highly-branched differentiated oligodendrocytes consisting of a small population of newborn mouse brain cell cultures (Fig. 2, panels d–f).

Finally, we studied coexpression of Nogo-A and CNP *in vivo* in the human brain by immunohistochemistry. A substantial overlap was found in the expression pattern of Nogo-A, NIG and CNP in oligodendrocytes and myelin sheaths of the cerebral white matter (Fig. 2, panels g and h), supporting the possibility that Nogo-A *in vivo* interacts with CNP, probably by binding via the NIG domain.

DISCUSSION

Protein microarray serves as a powerful tool for the rapid and systematic identification of protein-protein and other biomolecule interactions.[10] Protein microarray has a wide range of applications, including characterization of antibody specificity and autoantibody repertoire, and identification of novel biomarkers and molecular targets associated with disease type, stage and progression, leading to establishment of personalized medicine.[10] When a specific probe is available, the whole experimental procedure of protein microarray analysis requires the exact time shorter than 5 h to obtain the complete list of interacting proteins on the array.[11,12]

However, protein microarray technology is still under development in methodological aspects.[10–12] In general, protein microarray has its own limitations associated with the expression and purification of a wide variety of target proteins. In the microarray we utilized, the target proteins were expressed in a baculovirus expression system, purified under native conditions, and spotted on the slides to ensure the preservation of native structure, post-translational modifications such as glycosylation and phophorylation, and proper functionality. In contrast, bacterially expressed proteins lack glycosylation and phosphorylation moieties, and are often misfolded during purification. Since target proteins contain a GST fusion tag, the arrays are always processed for the post-spotting quality control by using an anti-GST antibody with a concentration gradient of GST spots as a standard. This procedure makes it possible to quantify the exact amount of proteins deposited in each spot, and thereby minimizes the inter-lot variability of the results. Furthermore, each subarray contains a series of built-in control spots.

Protein microarray also has another technical limitation attributable to the avidity of protein-protein interaction.[10–12] The probing and rigorous washing procedure detects mostly the direct protein-protein interaction supported by the stable binding ability. It could not efficiently detect much weak and transient protein-protein interactions, or indirect interactions that require accessory molecules or intervening cofactors. In addition,

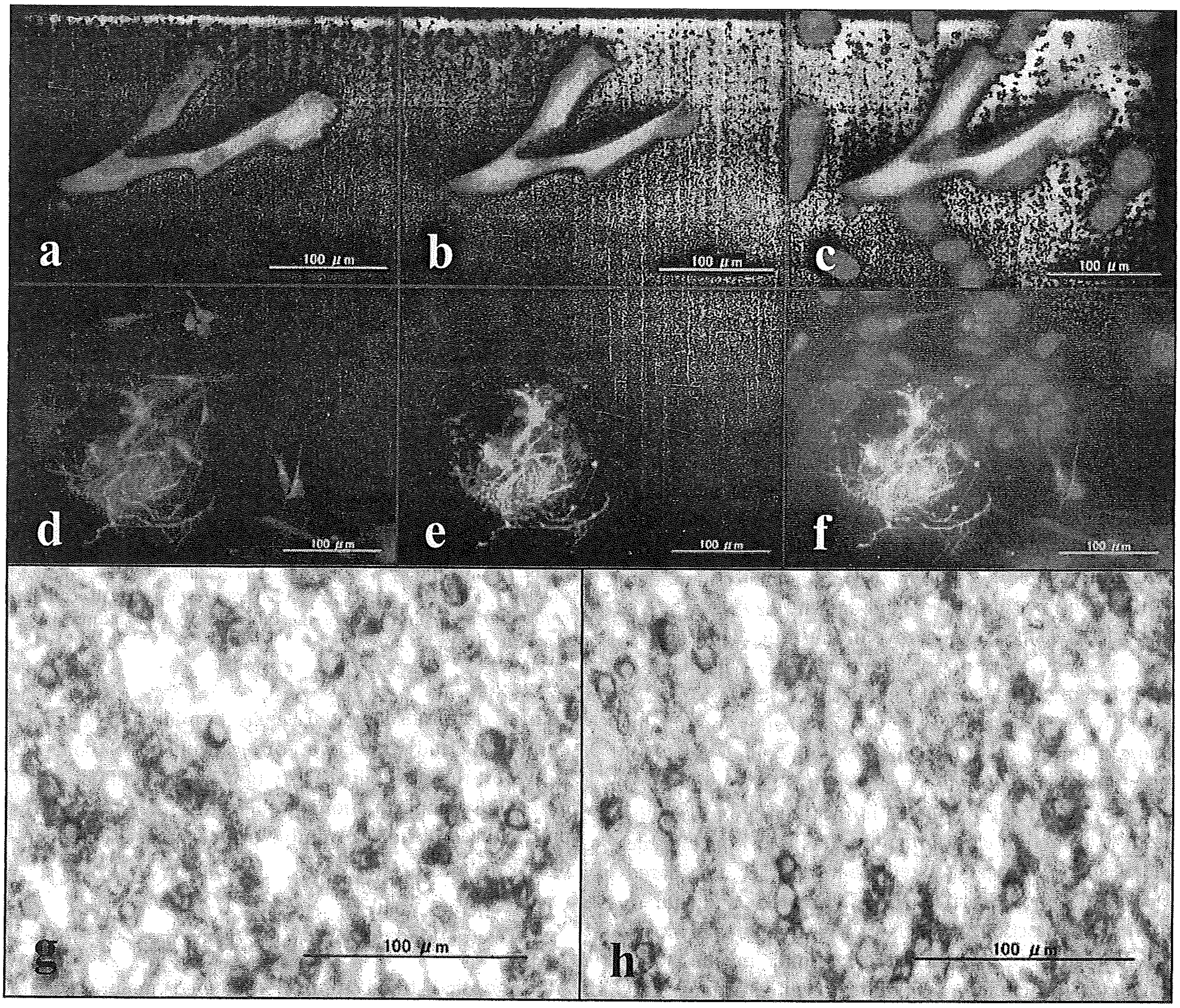

Fig. 2 Coexpression of NIG and anti-2′, 3′-cyclic nucleotide 3′-phosphodiesterase (CNP). (a–c) SK-N-SH neuroblastoma cells. The NIG gene and the CNP gene were cloned into the expression vectors to express a fusion protein with a DsRed or Halo tag, and they were cotransfected in SK-N-SH cells. (a) DsRed-labeled NIG, (b) Oregon Green-labeled CNP, and (c) merge (a) and (b) with 4′, 6′-diamidino-2-phenylindole (DAPI). (d–f) Newborn mouse brain cell cultures. Primary cultures established from newborn ICR mice double immunolabeled with anti-NIG antibody (AF3515) and anti-CNP antibody (11-5B), followed by labeling with Alexa Fluor 568-conjugated anti-sheep IgG and Alexa Fluor 488-conjugated anti-mouse IgG. (d) NIG, (e) CNP, and (f) merge (d) and (e) with DAPI. (g,h) Human brain tissues. The human brain tissue section derived from the peri-infarct white matter of the frontal cortex of a 62-year-old male with middle cerebral artery occlusion was double immunolabeled with (g) anti-Nogo-A antibody (H-300; brown) and anti-CNP antibody (11-5B; red) and (h) anti-NIG antibody (AF3515; brown) and anti-CNP antibody (11-5B; red).

protein microarray screening does not consider the specific subcellular location where the protein-protein interaction actually takes place. Thus, it is possible that some promiscuous partners are detected, whereas some biologically important interactors *in vivo* are left beyond identification. Therefore, protein microarray data always require the validation by other independent methods such as coimmunoprecipitation, Western blotting, the yeast two-hybrid (Y2H) screening, and so on. Post-translational modifications play a pivotal role in a range of protein-protein interactions. Immunolabeling of the array we utilized with anti-phosphotyrosine antibody showed that approximately 10–20% of the proteins on the array are phosphorylated (unpublished data of Invitrogen). When the array was applied for kinase substrate identification, most known kinases immobilized on the array are enzymatically active with the capacity of autophosphorylation, suggesting that they are functionally active with preservation of proper conformation (unpublished data of Invitrogen).

Previous studies indicate that the central domain of Amino-Nogo spanning amino acids 567–748 in the human Nogo-A designated NIG mediates persistent inhibition of axonal outgrowth and induces growth cone collapse by signaling through an as yet unidentified NIG receptor.[3] To characterize NIG-interacting proteins that might include an NIG receptor, we screened the high-density human protein microarray composed of 5000 proteins with a recombinant NIG protein as a probe. However, most of the 82 NIG interactors identified by protein microarray analysis are non-neural proteins, suggesting promiscuous binding in a non-physiological setting on the array. Therefore, we focused exclusively on the proteins whose expression in the CNS is supported by the expression profiling on UniGene, HRPD and ABA databases. Subsequently, we searched them on PubMed and retrieved 12 neuron/oligodendrocyte-associated NIG interactors (Table 1). Among them, we finally identified CNP as the most probable candidate in view of a physiological relevance to axon, myelin and oligodendrocytes. CNP is a valid cell type-specific marker for oligodendrocytes, essential for axonal support but not for myelin assembly.[15] CNP acts as a membrane anchor for tubulin required for process outgrowth of oligodendrocytes,[16,17] and ubiquitinated CNP is concentrated within lipid rafts,[18] suggesting that CNP expressed intracellularly in the cytoplasm is located in close proximity to the cell membrane where Nogo-A is accumulated. Therefore, we considered CNP as the most feasible NIG interactor candidate *in vivo*. The interaction of NIG with CNP and their coexpression in both oligodendrocytes and myelin were validated by immunoprecipitation, cell imaging, and immunolabeling.

Previously, we and others showed that Nogo-A expression is greatly enhanced in surviving oligodendrocytes and CNP is expressed in damaged but still remaining myelin sheaths, while NgR is upregulated in reactive astrocytes and macrophages/microglia at the edge of chronic active demyelinating lesions of multiple sclerosis (MS),[19,20] suggesting a pathological role of Nogo-A/NgR interaction in persistent demyelination and loss of axonal regeneration in MS lesions. Interestingly, a certain population of MS patients shows enhanced T-cell and B-cell responses against CNP and Nogo-A, suggesting that both CNP and Nogo-A serve as autoantigens.[21,22] Nogo-A takes at least two different membrane topologies in oligodendrocytes,[3,8] where it is possible that the N-terminal region of Nogo-A is exposed to the extracellular space or is located in the cytoplasm. Because CNP is expressed primarily in the cytoplasm of oligodendrocytes, it might not serve as a cell-surface NIG receptor possibly expressed on axons and

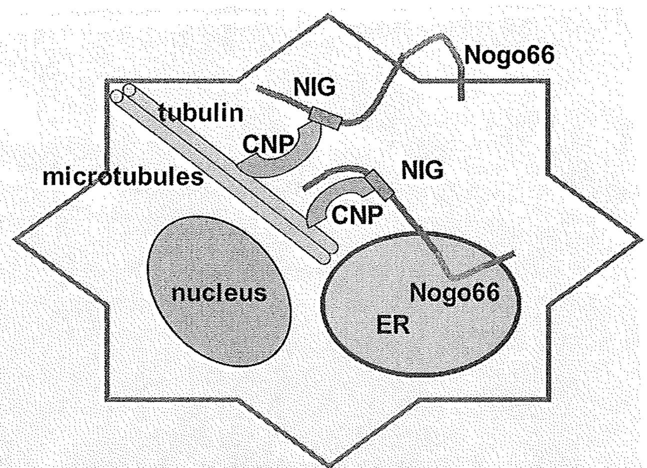

Fig. 3 A hypothetical model of NIG and anti-2′, 3′-cyclic nucleotide 3′-phosphodiesterase (CNP) interaction in oligodendrocytes. CNP (the orange piece) acts as a membrane anchor for tubulin essential for process outgrowth of oligodendrocytes, located in close proximity to the plasma membrane and possibly to the ER membrane where Nogo-A is accumulated. By interacting with NIG (the grey box), CNP serves as an intracellular conformational stabilizer for the intrinsically unstructured large segment of Amino-Nogo.

neurons that transduces the signals for inhibition of axonal outgrowth and induction of growth cone collapse. However, the possibility exists that CNP could act as an intracellular conformational stabilizer for the intrinsically-unstructured unstable Amino-Nogo segment in oligodendrocytes (Fig. 3).

ACKNOWLEDGMENTS

All autopsied brain samples obtained under written informed consent were provided by Research Resource Network (RRN), Japan. This work was supported by a research grant to J-IS from the High-Tech Research Center Project, the Ministry of Education, Culture, Sports, Science and Technology (MEXT), Japan (S0801043).

REFERENCES

1. Walmsley AR, Mir AK. Targeting the Nogo-a signalling pathway to promote recovery following acute CNS injury. *Curr Pharm Des* 2007; **13**: 2470–2484.
2. Pernet V, Joly S, Christ F, Dimou L, Schwab ME. Nogo-A and myelin-associated glycoprotein differently regulate oligodendrocyte maturation and myelin formation. *J Neurosci* 2008; **28**: 7435–7444.
3. Oertle T, van der Haar ME, Bandtlow CE *et al.* Nogo-A inhibits neurite outgrowth and cell spreading with three discrete regions. *J Neurosci* 2003; **23**: 5393–5406.

4. Li M, Song J. The N- and C-termini of the human Nogo molecules are intrinsically unstructured: bioinformatics, CD, NMR characterization, and functional implications. *Proteins* 2007; **68**: 100–108.
5. Zander H, Hettich E, Greiff K, Chatwell L, Skerra A. Biochemical characterization of the recombinant human Nogo-A ectodomain. *FEBS J* 2007; **274**: 2603–2613.
6. Schweigreiter R, Walmsley AR, Niederöst B *et al.* Versican V2 and the central inhibitory domain of Nogo-A inhibit neurite growth via p75NTR/NgR-independent pathways that converge at RhoA. *Mol Cell Neurosci* 2004; **27**: 163–174.
7. Freund P, Schmidlin E, Wannier T *et al.* Nogo-A-specific antibody treatment enhances sprouting and functional recovery after cervical lesion in adult primates. *Nat Med* 2006; **12**: 790–792.
8. Dodd DA, Niederoest B, Bloechlinger S, Dupuis L, Loeffler JP, Schwab ME. Nogo-A, -B, and -C are found on the cell surface and interact together in many different cell types. *J Biol Chem* 2005; **280**: 12494–12502.
9. Hu F, Strittmatter SM. The N-terminal domain of Nogo-A inhibits cell adhesion and axonal outgrowth by an integrin-specific mechanism. *J Neurosci* 2008; **28**: 1262–1269.
10. Schweitzer B, Predki P, Snyder M. Microarrays to characterize protein interactions on a whole-proteome scale. *Proteomics* 2003; **3**: 2190–2199.
11. Satoh J, Nanri Y, Yamamura T. Rapid identification of 14-3-3-binding proteins by protein microarray analysis. *J Neurosci Methods* 2006; **152**: 278–288.
12. Satoh J, Obayashi S, Misawa T, Sumiyoshi K, Oosumi K, Tabunoki H. Protein microarray analysis identifies human cellular prion protein interactors. *Neuropathol Appl Neurobiol* 2009; **35**: 16–35.
13. Voeltz GK, Prinz WA, Shibata Y, Rist JM, Rapoport TA. A class of membrane proteins shaping the tubular endoplasmic reticulum. *Cell* 2006; **124**: 573–586.
14. Lein ES, Hawrylycz MJ, Ao N *et al.* Genome-wide atlas of gene expression in the adult mouse brain. *Nature* 2007; **445**: 168–176.
15. Lappe-Siefke C, Goebbels S, Gravel M *et al.* Disruption of Cnp1 uncouples oligodendroglial functions in axonal support and myelination. *Nat Genet* 2003; **33**: 366–374.
16. Bifulco M, Laezza C, Stingo S, Wolff J. 2′,3′-Cyclic nucleotide 3′-phosphodiesterase: a membrane-bound, microtubule-associated protein and membrane anchor for tubulin. *Proc Natl Acad Sci USA* 2002; **99**: 1807–1812.
17. Lee J, Gravel M, Zhang R, Thibault P, Braun PE. Process outgrowth in oligodendrocytes is mediated by CNP, a novel microtubule assembly myelin protein. *J Cell Biol* 2005; **170**: 661–673.
18. Hinman JD, Chen CD, Oh SY, Hollander W, Abraham CR. Age-dependent accumulation of ubiquitinated 2′, 3′-cyclic nucleotide 3′-phosphodiesterase in myelin lipid rafts. *Glia* 2008; **56**: 118–133.
19. Satoh J, Onoue H, Arima K, Yamamura T. Nogo-A and nogo receptor expression in demyelinating lesions of multiple sclerosis. *J Neuropathol Exp Neurol* 2005; **64**: 129–138.
20. Kuhlmann T, Remington L, Maruschak B, Owens T, Brück W. Nogo-A is a reliable oligodendroglial marker in adult human and mouse CNS and in demyelinated lesions. *J Neuropathol Exp Neurol* 2007; **66**: 238–246.
21. Muraro PA, Kalbus M, Afshar G, McFarland HF, Martin R. T cell response to 2′,3′-cyclic nucleotide 3′-phosphodiesterase (CNPase) in multiple sclerosis patients. *J Neuroimmunol* 2002; **130**: 233–242.
22. Onoue H, Satoh JI, Ogawa M, Tabunoki H, Yamamura T. Detection of anti-Nogo receptor autoantibody in the serum of multiple sclerosis and controls. *Acta Neurol Scand* 2007; **115**: 153–160.

SUPPORTING INFORMATION

Additional Supporting Information may be found in the online version of this article:

Table S1 The complete list of the proteins immobilized on a human protein microarray utilized in the present study
Table S2 The list of 82 NIG interactors identified by protein microarray

Please note: Wiley-Blackwell are not responsible for the content or functionality of any supporting materials supplied by the authors. Any queries (other than missing material) should be directed to the corresponding author for the article.

Cell Mol Neurobiol
DOI 10.1007/s10571-009-9466-3

ORIGINAL RESEARCH

Stable Expression of Neurogenin 1 Induces LGR5, a Novel Stem Cell Marker, in an Immortalized Human Neural Stem Cell Line HB1.F3

Jun-ichi Satoh · Shinya Obayashi · Hiroko Tabunoki · Taeko Wakana · Seung U. Kim

Received: 15 August 2009 / Accepted: 25 September 2009

Abstract Neural stem cells (NSC) with self-renewal and multipotent properties serve as an ideal cell source for transplantation to treat spinal cord injury, stroke, and neurodegenerative diseases. To efficiently induce neuronal lineage cells from NSC for neuron replacement therapy, we should clarify the intrinsic genetic programs involved in a time- and place-specific regulation of human NSC differentiation. Recently, we established an immortalized human NSC clone HB1.F3 to provide an unlimited NSC source applicable to genetic manipulation for cell-based therapy. To investigate a role of neurogenin 1 (Ngn1), a proneural basic helix-loop-helix (bHLH) transcription factor, in human NSC differentiation, we established a clone derived from F3 stably overexpressing Ngn1. Genome-wide gene expression profiling identified 250 upregulated genes and 338 downregulated genes in Ngn1-overexpressing F3 cells (F3-Ngn1) versus wild-type F3 cells (F3-WT). Notably, leucine-rich repeat-containing G protein-coupled receptor 5 (LGR5), a novel stem cell marker, showed an 167-fold increase in F3-Ngn1, although transient overexpression of Ngn1 did not induce upregulation of LGR5, suggesting that LGR5 is not a direct transcriptional target of Ngn1. KeyMolnet, a bioinformatics tool for analyzing molecular relations on a comprehensive knowledgebase, suggests that the molecular network of differentially expressed genes involves the complex interaction of networks regulated by multiple transcription factors. Gene ontology (GO) terms of development and morphogenesis are enriched in upregulated genes, while those of extracellular matrix and adhesion are enriched in downregulated genes. These results suggest that stable expression of a single gene Ngn1 in F3 cells induces not simply neurogenic but multifunctional changes that potentially affect the differentiation of human NSC via a reorganization of complex gene regulatory networks.

Keywords HB1.F3 · KeyMolnet · LGR5 · Microarray · Neural stem cells · Neurogenin 1

Electronic supplementary material The online version of this article (doi:10.1007/s10571-009-9466-3) contains supplementary material, which is available to authorized users.

J. Satoh (✉) · S. Obayashi · H. Tabunoki · T. Wakana
Department of Bioinformatics and Molecular Neuropathology, Meiji Pharmaceutical University, 2-522-1 Noshio, Kiyose, Tokyo 204-8588, Japan
e-mail: satoj@my-pharm.ac.jp

S. U. Kim
Division of Neurology, Department of Medicine, University of British Columbia Hospital, University of British Columbia, Vancouver, BC, Canada

S. U. Kim
Medical Research Institute, Chung-Ang University College of Medicine, Seoul, Korea

Published online: 08 October 2009

Abbreviations

bHLH	Basic helix-loop-helix
CNS	Central nervous system
DAVID	Database for annotation visualization and integrated discovery
DEG	Differentially expressed genes
FBS	Fetal bovine serum
GAS2	Growth arrest-specific 2
GO	Gene ontology
HAS2	Hyaluronan synthase 2
LGR5	Leucine-rich repeat-containing G protein-coupled receptor 5
MMP9	Matrix metallopeptidase 9
Ngn1	Neurogenin 1

NPC	Neural progenitor cells
NSC	Neural stem cells
ORF	Open-reading frame
RMA	Robust multiarray average
RT-PCR	Reverse transcription-polymerase chain reaction
SHH	Sonic hedgehog homolog
Wnt	Wingless-type MMTV integration site family

Introduction

Neural stem cells (NSC) with self-renewal and multipotent properties serve as an ideal cell source for transplantation to treat spinal cord injury, stroke, and neurodegenerative diseases (Kim 2004; Kim and de Vellis 2009). To efficiently induce neuronal lineage cells from NSC for neuron replacement therapy, we should clarify the intrinsic genetic programs involved in a time- and place-specific regulation of human NSC differentiation. Previously, we found that primary cultures of human neural progenitor cells (NPC) exhibit an intrinsic capacity to differentiate into astrocytes in response to bone morphogenic protein 4 (BMP4) included in the serum (Obayashi et al. 2009). This might be a major hindrance against the proper commitment to neuronal linage cells following transplantation of NSC in vivo. Recently, we established an immortalized human NSC clone HB1.F3 by retroviral vector-mediated v-myc gene transfer into fetal human telencephalon cell cultures (Kim 2004). HB1.F3 cells could provide an unlimited NSC source applicable to genetic manipulation ex vivo for cell-based therapy. Actually, F3 cells stably expressing therapeutic genes migrate and integrate into target brain tissues upon transplantation in animal models of Parkinson disease, Huntington disease, and amyotrophic lateral sclerosis, and they differentiate into neurons, followed by an enhanced functional recovery (Kim et al. 2006; Kim and de Vellis 2009).

Neurogenin-1 (NEUROG1, Ngn1) is a member of proneural basic helix-loop-helix (bHLH) transcription factors that promote neurogenesis by activating a battery of target genes, including the NeuroD family of bHLH transcription factors (Morrison 2001). During embryogenesis, Ngn1 is expressed in NPC distributed in dorsal root ganglia (DRG), dorsal and ventral regions of the neural tube, dorsal telencephalon, and specific regions within the midbrain and hindbrain (Sommer et al. 1996). Although there exists a functional redundancy among Ngn1, Ngn2, and Ngn3, Ngn1-deficient mice failed to generate a $TrkA^{+}$ subset of cervical DRG neurons (Ma et al. 1999). Overexpression of Ngn1 induces neurite outgrowth in F11 rat DRG and mouse neuroblastoma hybrid cells (Kim et al. 2002). Stable expression of Ngn1 induces neuronal differentiation of pluripotent mouse embryonal carcinoma P19 cells (Kim et al. 2004). Ngn1 inhibits differentiation of rat NSC into astrocytes by sequestering a transcriptional coactivator complex composed of CBP and SMAD1 and blocking activation of STAT transcription factors (Sun et al. 2001).

In the present study, to investigate the role of Ngn1 in human NSC differentiation, we established a clonal cell line stably overexpressing Ngn1 by retroviral vector-mediated gene transfer into HB1.F3 cells. Then, we studied genome-wide gene expression profiles of Ngn1-overexpressing F3 cells (F3-Ngn1) and wild-type F3 cells (F3-WT) by using whole genome DNA microarrays. As a result, we unexpectedly found that stable expression of a single gene Ngn1 in F3 cells induced a robust upregulation of leucine-rich repeat-containing G protein-coupled receptor 5 (LGR5), a recently identified marker for intestine and hair follicle stem cells (Barker et al. 2007; Jaks et al. 2008; Sato et al. 2009). Our results suggested that stable expression of Ngn1 in human NSC cells induces not only simply neurogenic but also multifunctional changes that potentially affect the differentiation of NSC via a reorganization of complex gene regulatory networks.

Methods

Human Neural Stem Cell Clone HB1.F3 and Its Derivative HB1.F3-Ngn1

Primary cultures of fetal human telencephalon cells were transformed with a retroviral vector pLSNmyc carrying the v-myc oncogene and the neomycin resistance gene. Following selection with G418, a single continuously dividing clone with a capacity to self-renew and differentiate into neurons and glial cells both in vitro and in vivo was isolated and designated HB1.F3 (Kim 2004). It carried normal human karyotype of 46 XX. After transducing a retroviral vector pBabePNgn1 carrying the open-reading frame (ORF) of the human Ngn1 gene and the puromycin resistance gene into HB1.F3 cells, a single puromycin-resistant clone was selected, expanded, and designated HB1.F3-Ngn1. In the present study, the wild-type HB1.F3 cells and the HB1.F3-Ngn1 cells are abbreviated as F3-WT and F3-Ngn1. They were incubated in the feeding medium composed of Dulbecco's modified Eagle's medium (DMEM) (Invitrogen, Carlsbad, CA, USA) supplemented with 10% fetal bovine serum (FBS), 100 U/ml penicillin and 100 μg/ml streptomycin. The medium was renewed every 3 days.

Microarray Analysis

Total RNA was isolated from subconfluent cells by using the TRIZOL Plus RNA Purification kit (Invitrogen). The quality of total RNA was evaluated on Agilent 2100 Bioanalyzer (Agilent Technologies, Palo Alto, CA, USA). One hundred nanograms of total RNA was processed for cRNA synthesis, fragmentation, and terminal labeling with the GeneChip Whole Transcript Sense Target Labeling and Control Reagents (Affymetrix, Santa Clara, CA, USA). Then, it was processed for hybridization at 45°C for 17 h with Human Gene 1.0 ST Array (Affymetrix) containing 28,869 genes with approximately 26 probes per each gene that spread across the full length of the gene. The arrays were washed in the GeneChip Fluidic Station 450 (Affymetrix), and scanned by the GeneChip Scanner 3000 7G (Affymetrix). The data expressed as CEL files were normalized by the robust multiarray average (RMA) method with the Expression Console software version 1.1 (Affymetrix). By comparing the signal intensity levels between F3-WT and F3-Ngn1, the genes exhibiting either greater than twofold upregulation or smaller than 0.5-fold downregulation are considered as differentially expressed genes (DEG). To perform unsupervised clustering analysis of gene expression profiles, the CEL file-based data were imported to GeneSpring GX10 (Agilent).

Molecular Network Analysis

KeyMolnet is a comprehensive knowledgebase, originally established by the Institute of Medicinal Molecular Design (IMMD), Tokyo, Japan (Sato et al. 2005). It contains numerous contents of human genes, molecules and molecular relations, diseases, pathways, and drugs, all of which are manually collected, carefully curated, and regularly updated by expert biologists. The database is categorized into the core contents collected from selected review articles with the highest reliability or the secondary contents extracted from abstracts of PubMed database and Human Protein Reference database (HPRD). By importing the list of Entrez Gene ID and signal intensity data, KeyMolnet automatically provides corresponding molecules as a node on networks. Among various network-searching algorithms, the "N-points to N-points" search extracts the molecular network with the shortest route connecting the starting point molecules and the end point molecules. The generated network was compared side by side with 403 human canonical pathways of the KeyMolnet library. The algorithm counting the number of overlapping molecular relations between the extracted network and the canonical pathway makes it possible to identify the canonical pathway showing the most significant contribution to the extracted network. The significance in the similarity between both is scored following the formula, where O = the number of overlapping molecular relations between the extracted network and the canonical pathway, V = the number of molecular relations located in the extracted network, C = the number of molecular relations located in the canonical pathway, T = the number of total molecular relations composed of approximately 110,000 sets, and the X = the sigma variable that defines coincidence.

$$\text{Score} = -\log_2(\text{Score (p)}) \quad \text{Score(p)} = \sum_{x=O}^{\text{Min}(C,V)} f(x)$$

$$f(x) = {}_C C_x \cdot {}_{T-C} C_{V-x} / {}_T C_V$$

Gene Annotation Analysis

Functional annotation of differentially expressed genes was searched by the web-accessible program named Database for Annotation, Visualization, and Integrated Discovery (DAVID) version 2008, National Institute of Allergy and Infectious Diseases (NIAID), NIH (david.abcc.ncifcrf.gov) (Huang da et al. 2009). It covers more than 40 annotation categories, including Gene ontology (GO) terms, protein–protein interactions, protein functional domains, disease associations, biological pathways, sequence general features, homologies, gene functional summaries, and tissue expressions. By importing the list of Entrez Gene ID, this program creates the functional annotation chart, an annotation-term-focused view that lists annotation terms and their associated genes under study. To avoid excessive counting of duplicated genes, the Fisher Exact statistics is calculated based on corresponding DAVID gene IDs by which all redundancies in original IDs are removed.

Real-Time RT-PCR Analysis

DNase-treated total cellular RNA was processed for cDNA synthesis using oligo(dT)$_{12-18}$ primers and SuperScript II reverse transcriptase (Invitrogen). Then, cDNA was amplified by PCR in LightCycler ST300 (Roche Diagnostics, Tokyo, Japan) using SYBR Green I and primer sets listed in Table 1. The expression levels of target genes were standardized against those of the glyceraldehyde-3-phosphate dehydrogenase (G3PDH) gene detected in parallel in identical cDNA samples. All the assays were performed in triplicate.

In some experiments, the ORF of Ngn1 was amplified by PCR using PfuTurbo DNA polymerase (Stratagene, La Jolla, CA, USA) and primer sets listed in Table 1. It was then cloned into the mammalian expression vector p3XFLAG-CMV7.1 (Sigma, St. Louis, MO, USA) to express a fusion protein with an N-terminal Flag tag. At 48 h after transfection of the vector in F3-WT cells by Lipofectamine 2000 reagent (Invitrogen), the cells were processed for real-time RT-PCR analysis of LGR5 and Western blot analysis of a Flag-fusion protein with anti-Flag M2 antibody (Sigma).

Table 1 Primers for RT-PCR and cloning utilized in the present study

Genes	GenBank accession no.	Sense primers	Antisense primers
NES	NM_006617	5′ctgctcaggagcagcactcttaac3′	5′cttagcctatgagatggagcaggc3′
LGR5	NM_003667	5′aacagtcctgtgactcaactcaag3′	5′ttagagacatgggacaaatgccac3′
GAS2	NM_005256	5′acaaacatgtcatggtccgtgtgg3′	5′aactggcagagaccaccaagtagt3′
HAS2	NM_005328	5′gccagctgccttagaggaaatatc3′	5′atggttttccttcctgatgtgccc3′
MMP9	NM_004994	5′tcttccagtaccgagagaaagcct3′	5′ctgcaggatgtcataggtcacgta3′
NEUROG1	NM_006161	5′ttcctcaccgacgaggaagactgt3′	5′tcaagttgtgcatgcggttgcgct3′
NEUROG1 for cloning	NM_006161	5′cggaattccccagcccgccttgagacctgc3′	5′cgggatcccgctagtggtaaggaatgaaac3′
G3PDH	NM_002046	5′ccatgttcgtcatgggtgtgaacca3′	5′gccagtagaggcagggatgatgttc3′

NES Nestin, *LGR5* leucine-rich repeat-containing G protein-coupled receptor 5, *GAS2* growth arrest-specific 2, *HAS2* hyaluronan synthase 2, *MMP9* matrix metallopeptidase 9, *NEUROG1* neurogenin 1, and *G3PDH* glyceraldehyde-3-phosphate dehydrogenase

Western Blot Analysis

To prepare total protein extract, the cells were homogenized in RIPA buffer containing a cocktail of protease inhibitors (Sigma). After separation on a 12% SDS-PAGE gel, the protein was transferred onto a nitrocellulose membrane, and the blot was incubated with rabbit polyclonal anti-LGR5 antibody (AP2745d) (ABGENT, Flanders Court, San Diego, CA, USA). Then, it was labeled with HRP-conjugated anti-rabbit IgG (Santa Cruz Biotechnology, Santa Cruz, CA, USA). The specific reaction was visualized by exposing of the blot to a chemiluminescence substrate (Pierce, Rockford, IL, USA). After the antibodies were stripped by incubating the membrane at 50°C for 30 min in stripping buffer, composed of 62.5 mM Tris–HCl, pH 6.7, 2% SDS, and 100 mM 2-mercaptoethanol, it was processed for relabeling with anti-Hsp60 antibody (N-20; Santa Cruz Biotechnology), an internal control for protein loading.

Results

Overexpression of Neurogenin 1 in F3-Ngn1 Cells

When incubated in the feeding medium, both F3-WT and F3-Ngn1 cells proliferated continuously with a doubling time ranging from 3 to 7 days. Although they were morphologically different, i.e. F3-WT exhibited a fusiform morphology, while F3-Ngn1 exhibited a cuboidal appearance (Fig. 1A, panels a and b), both of them expressed nestin but did not form a neurosphere when cultured in the feeding medium. The levels of expression of nestin mRNA were higher in F3-Ngn1 than F3-WT (Fig. 1B, panel a, lanes 1 and 2). Importantly, only F3-Ngn1 expressed Ngn1 mRNA (Fig. 1B, panel b, lanes 1 and 2).

We conducted genome-wide gene expression profiling of F3-WT and F3-Ngn1 by using two sets of Human Gene 1.0 ST Array for each, followed by two comparisons composed of F3-WT array-1 (WT-1) versus F3-Ngn1 array-1 (NGN-1) and F3-WT array-2 (WT-2) versus F3-Ngn1 array-2 (NGN-2). Unsupervised clustering analysis of these data clearly separated the cluster of F3-Ngn1 from that of F3-WT, based on gene expression profiles of 59 genes differentially expressed between both cell types (Fig. 2). The gene expression profile of WT-1 was similar to that of WT-2, while the gene expression profiles of NGN-1 and NGN-2 were almost identical, supporting the reproducibility among the results of repeated microarray analysis (Fig. 2). The analysis of individual probe data identified significant upregulation of Ngn1 ORF expression

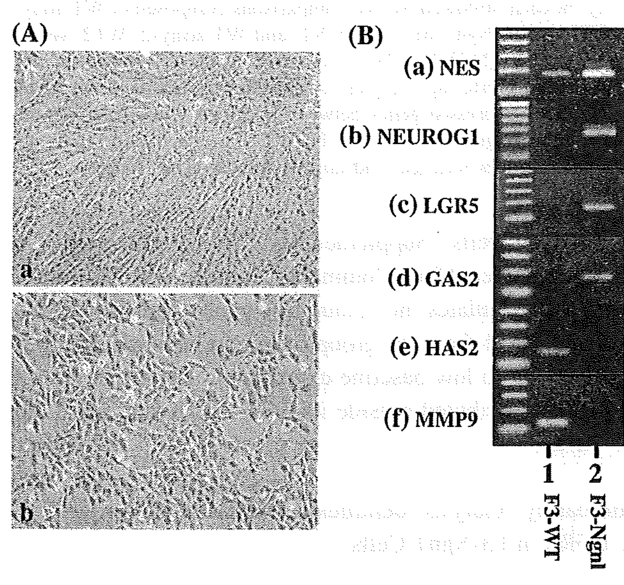

Fig. 1 Characterization of phenotypes of F3-WT and F3-Ngn1 cells. **A** Phase contrast photomicrograph. Both F3-WT cells (panel *a*) and F3-Ngn1 cells (panel *b*) were incubated in the feeding medium at a subconfluent density. **B** RT-PCR analysis. cDNA prepared from F3-WT cells (lane 1) and F3-Ngn1 cells (lane 2) was amplified by PCR for 30 cycles using primer sets listed in Table 1. The panels (*a*–*f*) represent (*a*) nestin (NES), (*b*) neurogenin 1 (NEUROG1), (*c*) leucine-rich repeat-containing G protein-coupled receptor 5 (LGR5), (*d*) growth arrest-specific 2 (GAS2), (*e*) hyaluronan synthase 2 (HAS2), and (*f*) matrix metallopeptidase 9 (MMP9)

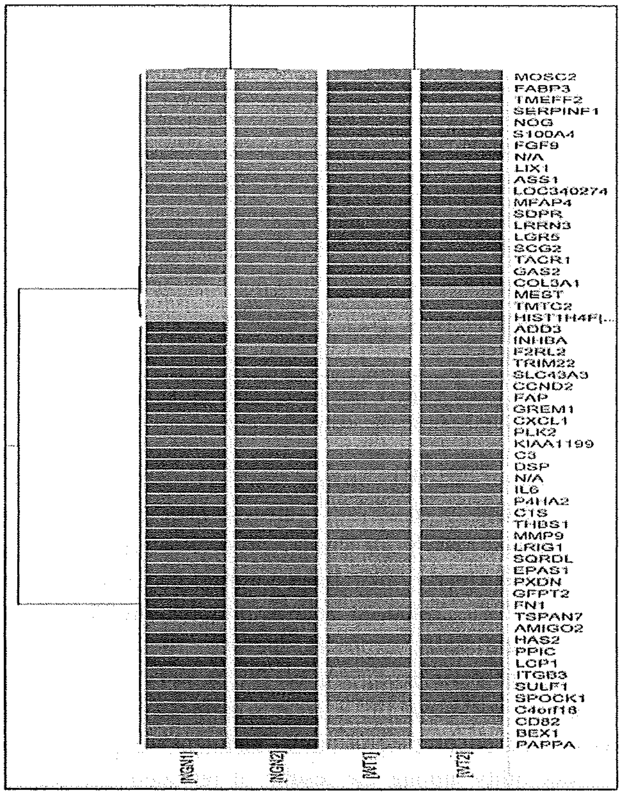

Fig. 2 Clustering analysis of gene expression profiles of F3-WT and F3-Ngn1 cells. Genome-wide gene expression profiling of F3-WT and F3-Ngn1 was performed by using two sets of Human Gene 1.0 ST Array for each, followed by two comparisons composed of WT array-1 (WT1) versus Ngn1 array-1 (NGN1) and WT array-2 (WT2) versus Ngn1 array-2 (NGN2). The microarray data are processed for unsupervised clustering analysis on GeneSpring GX10. A set of 59 differentially expressed genes between both cell types separated the cluster of F3-Ngn1 from that of F3-WT. The heat map represents upregulated genes (*orange*) and downregulated genes (*blue*)

in F3-Ngn1 cells (Supplementary Fig. 1). However, the Affymetrix GeneChip Command Console (AGCC) algorithm that calculates the cumulative gene expression levels excluded Ngn1 from the group of upregulated genes in F3-Ngn1 owing to low baseline expression of Ngn1 in the set of probes distributed outside its ORF on Human Gene 1.0 ST Array.

Microarray Analysis Identifies a Robust Induction of LGR5 in F3-Ngn1 Cells

Microarray analysis identified total 588 differentially expressed genes (DEG), composed of 250 upregulated genes and 338 downregulated genes in F3-Ngn1 versus F3-WT (see Supplementary Tables 1 and 2 for the complete lists). Top 20 upregulated genes are shown in Table 2. Notably, LGR5, a novel stem cell marker (Barker et al. 2007; Jaks et al. 2008; Sato et al. 2009), showed an 167-fold increase in F3-Ngn1 (Table 2; Fig. 3).

In view of cell type-specific markers for NSC, neurons, and glial cells, nestin (NES) exhibited a 3.1-fold increase in F3-Ngn1 (Supplementary Table 1; Fig. 3), consistent with RT-PCR results (Fig. 1B, panel a, lanes 1 and 2). However, the expression of other NSC-specific markers, such as musashi homolog 1 (MSI1) and ATP-binding cassette subfamily G member 2 (ABCG2), was not elevated in F3-Ngn1 (Fig. 3). Although neurofilament medium polypeptide (NEFM) showed a 2.1-fold increase, the expression of other neuron-specific markers, such as neurofilament heavy polypeptide (NEFH), enolase 2 (ENO2), and tubulin beta 3 (TUBB3), was not substantially upregulated in F3-Ngn1 (Fig. 3). The expression of astroglial (GFAP), oligodendroglial (MBP, MOG, and CNP), and microglial (CD68) markers remained unaltered (Fig. 3). Furthermore, NEUROD1, a putative Ngn-1 target gene,[5,10] was not upregulated in F3-Ngn1 (Fig. 3).

Top 20 downregulated genes are shown in Table 3. It is worthy to note that the great majority of top 20 downregulated genes are categorized as extracellular matrix-associated proteins.

RT-PCR and Western Blot Analysis Validated the Results of Microarray Analysis

Both the conventional RT-PCR and real-time RT-PCR analysis validated marked upregulation of LGR5 and GAS2, and remarkable downregulation of HAS2 and MMP9 in F3-Ngn1 (Fig. 1B, panels c–f, lanes 1 and 2; Fig. 4, panels a–d). Western blot analysis verified LGR5 protein expression exclusively in F3-Ngn1 (Fig. 4, panel e, lane 2).

To address the question whether LGR5 is a direct target for Ngn1, an expression vector of either Ngn1 or green fluorescent protein (GFP) was transfected in F3-WT cells (Fig. 5a, upper panel, lanes 1 and 2). At 48 h after transfection, the cells were processed for real-time RT-PCR analysis. Transient overexpression of Ngn1 did not induce LGR5 expression in F3-WT, suggesting that LGR5 is not a direct transcriptional target of Ngn1 (Fig. 5b).

An Involvement of the Complex Interaction of Networks Regulated by Multiple Transcription Factors in Development of F3-Ngn1 Cells

To clarify the molecular network of the genes differentially expressed between F3-WT and F3-Ngn1, we imported microarray data into KeyMolnet, a bioinformatics tool for analyzing molecular relations on a comprehensive knowledgebase. When Entrez Gene ID and expression levels of 588 DEG were imported, KeyMolnet recognized a set of 51 non-annotated genes to be removed. Then, it extracted 787